

BackPlay: Head-Only Look-Back Self-Correction for Diffusion Language Models*

Liming Liu, Binxuan Huang, Zixuan Zhang, Xin Liu, Bing Yin, Tuo Zhao

Abstract

Diffusion Language Models (DLMs) decode multiple tokens in parallel, but aggressive multi-token decoding amplifies cross-token dependency errors and can sharply degrade generation quality. We propose BackPlay, a frozen-backbone self-correction framework that trains only a lightweight correction head on a finetuned DLM without updating any backbone or adapter parameters. Because the head is trained on errors produced by the same frozen generator used at inference time, its training distribution aligns with the error patterns of the deployed model. We further introduce Look-back Correction, a training mechanism that injects predictions from earlier, more corrupted denoising states into later, richer contexts, enabling the head to leverage later context to detect mistakes made in earlier generation steps. During inference, BackPlay periodically revisits previously generated tokens through selective remasking and regeneration to limit error accumulation. Across mathematical reasoning and code generation benchmarks, BackPlay improves the speed-quality trade-off of the underlying DLM under multi-token decoding.

1 Introduction

Diffusion Language Models (DLMs) have emerged as a powerful alternative to autoregressive (AR) models for language generation, offering substantial speedups through parallel decoding (Sahoo et al., 2024; Nie et al., 2024; Ye et al., 2025; Zhu et al., 2025). Unlike AR models that generate tokens sequentially, DLMs start from a fully masked sequence and iteratively reveal tokens through a denoising process, producing multiple tokens simultaneously at each step. This parallel generation enables faster inference while achieving competitive performance across reasoning, coding, and planning tasks (Nie et al., 2025; Ye et al., 2025; Zhu et al., 2025).

The efficiency gains of parallel generation come with inherent challenges. When DLMs generate multiple tokens in the same iteration, particularly under aggressive multi-token decoding, they can amplify cross-token dependency errors (Liu et al., 2024; Xu et al., 2024; Kang et al., 2025). Errors introduced in early denoising steps may persist and propagate through subsequent iterations, degrading generation quality. This motivates self-correction mechanisms that can detect and rectify erroneous predictions during inference. In particular, tokens that appear locally plausible under sparse early context may become globally inconsistent as later denoising steps reveal richer surrounding information.

Self-correction methods for DLMs span a design space defined by several choices. Training-free approaches refine outputs via heuristic remasking or model-derived confidence scores (Wang et al., 2025; Zhao et al., 2024; Peng et al., 2025), but do not explicitly train a token-correctness predictor. Trainable approaches add a correction head that learns token-level error detection, with some methods jointly updating the generator alongside the head via a multi-objective loss (Huang et al., 2025; Kim et al., 2025). These methods differ along several design axes: whether the generator parameters are updated during corrector training, how artifact-containing training sequences are constructed, and whether the corrector explicitly leverages later denoising context to judge earlier predictions.

*Work done at Amazon. Correspondence to lliu606@amazon.com, lliu606@gatech.edu.

This paper targets a specific setting: a post-trained DLM is already available, and we wish to add inference-time self-correction without modifying the deployed generator. This motivates two design desiderata: (i) the corrector should train on a fixed generator to avoid distribution drift during head training, and (ii) the corrector should leverage later denoising context to revisit earlier predictions. In the head-based setup studied here, we empirically observe a fidelity–correction trade-off under joint optimization on the 1B model (Table 2), which means that simultaneously optimizing generation and correction objectives can degrade DLM’s generative capability. Moreover, preserving the deployed generator can be operationally preferable when the model has undergone substantial post-training.

Contributions: We propose BackPlay, a head-only self-correction framework for frozen finetuned DLMs. Our contributions are threefold:

First, we decouple corrector training from the generator. By freezing the finetuned DLM and training only a lightweight correction head—without updating backbone or adapter parameters—we avoid generator drift during head training and remove generator-side gradient computation by construction.

Second, we introduce Look-back Correction, a training mechanism that injects predictions from earlier, more corrupted denoising states into later, richer contexts, providing explicit later-context supervision for earlier errors. This enables the head to detect mistakes plausible under sparse context but inconsistent under richer later context.

Third, we show that BackPlay improves the speed–quality trade-off over the SFT baseline and internal ablations on mathematical reasoning and code generation benchmarks.

BackPlay is not the first trainable self-correction method for DLMs. Relative to PRISM (Kim et al., 2025) and RemeDi (Huang et al., 2025), our focus is a distinct operating regime: a frozen deployed generator, head-only training, and explicit later-context supervision for earlier errors. We summarize these design differences in Table 1 and detail them in Sections 3.1 and 3.2. Accordingly, this paper studies whether inference-time self-correction can be added to a post-trained DLM without updating the generator, while allowing the corrector to revisit earlier decisions under later context.

2 Preliminaries and Background on Trainable Self-Correction

2.1 Diffusion Language Models (DLMs)

Diffusion Language Models (DLMs) (Nie et al., 2024; 2025; Ye et al., 2025; Zhu et al., 2025) extend discrete diffusion (Austin et al., 2021; Lou et al., 2023; He et al., 2023; Sahoo et al., 2024; Gat et al., 2024; Shi et al., 2024) to language generation. A forward corruption process independently replaces tokens with a special mask token M , and the model is trained to recover the masked tokens from the remaining context.

Forward process. Let $\mathbf{x}_0 \in \mathcal{V}^L$ be a length- L clean sequence from dataset \mathcal{D} with vocabulary \mathcal{V} . For time $t \in [0, 1]$, the corrupted sequence $\mathbf{x}_t \in (\mathcal{V} \cup \{\mathsf{M}\})^L$ is obtained by independently masking each position:

$$q_{t|0}(\mathbf{x}_t|\mathbf{x}_0) = \prod_{i=1}^L q_{t|0}(x_t^i|x_0^i), \quad q_{t|0}(x_t^i|x_0^i) = \begin{cases} \alpha_t, & x_t^i = x_0^i, \\ 1 - \alpha_t, & x_t^i = \mathsf{M}. \end{cases}$$

Following standard practice, the linear schedule $\alpha_t = 1 - t$ is adopted, so that $t = 1$ yields a fully masked sequence.

Training. The model $p_\theta(\mathbf{x}_0|\mathbf{x}_t)$ is trained to predict original tokens at masked positions by minimizing the demasking loss:

$$\mathcal{L}_{\text{Demask}}(\theta) = \mathbb{E} \left[\frac{1}{t} \sum_{i: x_t^i = \mathsf{M}} -\log p_\theta(x_0^i | \mathbf{x}_t) \right], \quad (1)$$

where $t \sim \text{Unif}[0, 1]$, $\mathbf{x}_0 \sim \mathcal{D}$, and $\mathbf{x}_t \sim q_{t|0}(\cdot|\mathbf{x}_0)$.

Inference. Generation starts from a fully masked sequence $\mathbf{x}_1 = (\mathbb{M}, \dots, \mathbb{M})$ and proceeds over decreasing time steps $t_0=1 > \dots > t_N=0$. At each step, a subset of masked positions is selected and their tokens are sampled from $p_\theta(x_t^i \mid \mathbf{x}_{t_\ell})$. We refer to positions with $x_t^i \neq \mathbb{M}$ as *visible* and positions with $x_t^i = \mathbb{M}$ as *masked* in the following sections.

Because DLMs update multiple positions in parallel from the same partially observed state \mathbf{x}_t , the resulting tokens may violate cross-token dependencies even when each per-position prediction is locally plausible (Liu et al., 2024; Xu et al., 2024; Kang et al., 2025). This motivates correction mechanisms that evaluate visible tokens during denoising.

2.2 Self-Correction of DLMs

Training-free self-correction methods refine DLM outputs via heuristic remasking or model-derived confidence scores (Zhao et al., 2024; Wang et al., 2025; Peng et al., 2025), but are not directly trained against token correctness, which can limit calibration and systematic improvement. Trainable methods instead augment the DLM with a correction module that learns to predict per-token correctness from data (Huang et al., 2025; Kim et al., 2025).

Concretely, a correction module $\mathbf{g}_{\theta, \phi}(\mathbf{z}_t)$ takes a partially denoised sequence \mathbf{z}_t and, for each visible position i (i.e., $z_t^i \neq \mathbb{M}$), outputs a *correctness score*

$$c_i = \mathbf{g}_{\theta, \phi}(\mathbf{z}_t)_i \in [0, 1],$$

interpreted as $c_i \approx P(z_t^i = x_0^i \mid \mathbf{z}_t)$. At inference time, an equivalent *error score* $e_i := 1 - c_i$ can be used to rank candidates for remasking. The module is trained using Binary Cross-Entropy (BCE) loss over visible positions:

$$\mathcal{L}_{\text{Err}}(\theta, \phi) = \mathbb{E} \left[\sum_{i: z_t^i \neq \mathbb{M}} \text{BCE}(c_i, \mathbb{I}[z_t^i = x_0^i]) \right], \quad (2)$$

where $t \sim \text{Unif}[0, 1]$, $\mathbf{x}_0 \sim \mathcal{D}$, and $\mathbf{z}_t \sim q_{\text{sc}}(\cdot \mid \mathbf{x}_0, t)$. Masked positions ($z_t^i = \mathbb{M}$) contribute no loss, as there is no visible token to evaluate. Throughout this paper, correctness during training refers to exact agreement with the reference token x_0^i .

The central design problem is the choice of the self-correction training distribution $q_{\text{sc}}(\mathbf{z}_t \mid \mathbf{x}_0, t)$, which specifies how artifact-containing sequences \mathbf{z}_t are constructed. Here, q_{sc} denotes the distribution over artifact-containing sequences \mathbf{z}_t induced by the full construction pipeline, including artifact generation, position selection, and insertion. Prior methods start with a corrupted sequence $\mathbf{x}_t \sim q_{t|0}(\cdot \mid \mathbf{x}_0)$ and introduce artifact tokens $\mathbf{y} \sim P_{\text{artifact}}$ at selected positions \mathcal{M} :

$$\mathbf{z}_t = \text{replace}(\mathbf{x}_t, \mathbf{y}, \mathcal{M}), \quad \text{where} \quad [\text{replace}(\mathbf{x}_t, \mathbf{y}, \mathcal{M})]_i = \begin{cases} y^i, & \text{if } i \in \mathcal{M}, \\ x_t^i, & \text{otherwise.} \end{cases}$$

RemeDi (Huang et al., 2025) draws artifacts from a uniform distribution over the vocabulary \mathcal{V} , providing a simple control distribution that does not explicitly model structured, model-generated errors. PRISM (Kim et al., 2025) instead generates artifacts from the model’s own predictions at a slightly more corrupted state: given a step size Δt ,

$$\mathbf{x}_{t+\Delta t} \sim q_{t+\Delta t|0,t}(\cdot \mid \mathbf{x}_0, \mathbf{x}_t), \quad \mathbf{y} \sim p_\theta(\mathbf{x}_0 \mid \mathbf{x}_{t+\Delta t}),$$

and selects \mathcal{M} from newly unmasked positions—those masked in $\mathbf{x}_{t+\Delta t}$ but visible in \mathbf{x}_t —with $|\mathcal{M}| = \lceil L \cdot \Delta t \rceil$ to simulate one reverse-process transition. Both RemeDi and PRISM jointly optimize the generator and correction head:

$$\mathcal{L}(\theta, \phi) = \mathcal{L}_{\text{Demask}}(\theta) + \gamma \mathcal{L}_{\text{Err}}(\theta, \phi), \quad (3)$$

where γ balances the demasking and error-detection objectives.

These methods differ along three main axes: (a) whether generator-side parameters θ are updated during corrector training, (b) how the self-correction training distribution q_{sc} is constructed, and (c) whether earlier predictions are evaluated under later denoising context. These axes motivate the design considerations discussed next.

2.3 Design Motivation for Frozen-Backbone Self-Correction

Rather than claiming universal limitations of prior methods, we highlight three design considerations that motivate the operating point studied in this paper. In the setting considered here—a post-trained DLM that should remain unmodified—these considerations lead to a frozen-backbone, head-only correction design with explicit later-context supervision.

Preserving a deployed post-trained generator. When a DLM has undergone substantial supervised finetuning or post-training, it can be desirable to keep the generator parameters θ fixed and train only the correction head ϕ . In the head-based setup studied here, Table 2 in Section 4.1 provides evidence that joint optimization of θ and ϕ via Equation (3) can introduce a fidelity–correction trade-off on the 1B model.

Training the head on a fixed error source. When generator-side parameters are updated during head training, the artifact distribution seen by the head can evolve over the course of training. A frozen-generator design removes this source of drift by construction, so that the head trains on errors produced by the same fixed generator used at deployment.

Evaluating earlier decisions under later denoising context. Some early token decisions become identifiable as errors only after more context has been revealed in later denoising steps. Here, “look-back” refers to revisiting earlier denoising decisions under later denoising context; it is defined over the denoising timeline and is orthogonal to the semi-autoregressive block length used at inference. This motivates training recipes that reassess earlier predictions using richer later context.

These considerations define the operating point of BackPlay relative to prior trainable correctors. Our empirical evaluation in Section 4 focuses on controlled baselines and ablations within the frozen-backbone setting.

3 Method

Section 3.1 defines a head-only correction objective on a frozen deployed DLM. Section 3.2 constructs the Look-back Correction (LBC) training distribution that provides later-context supervision for earlier errors. Section 3.3 converts the learned correctness scores into a conservative remasking policy at inference time.

3.1 Head-Only Self-Correction on a Frozen Deployed DLM

Motivated by the design considerations in Section 2.3—preserving a deployed generator and training the head on a fixed error source—BackPlay treats the finetuned DLM as a frozen feature backbone and appends an auxiliary correction head ϕ , trained without any backbone or adapter modification, to predict the correctness of currently visible tokens.

Given a finetuned DLM with frozen parameters θ^* , we introduce a shallow Transformer correction head ϕ that operates on the penultimate-layer hidden states. Let N_L denote the number of layers in the frozen DLM. The correction head is defined as:

$$\mathbf{g}_{\theta^*,\phi}(\mathbf{z}_t) = \sigma\left(\phi(\mathbf{h}^{N_L-1})\right) \in [0, 1]^L, \quad (4)$$

where σ denotes the sigmoid function applied position-wise, and \mathbf{h}^{N_L-1} are the hidden states from the forward pass of $p_{\theta^*}(\mathbf{x}_0|\mathbf{z}_t)$. Since θ^* is fully frozen, the hidden-state distribution seen by ϕ does not change during head training, avoiding generator drift.

For each visible position i in the set $\mathcal{V}_t := \{j : z_t^j \neq \mathbb{M}\}$, the head outputs a correctness score $c_i = \mathbf{g}_{\theta^*,\phi}(\mathbf{z}_t)_i \in [0, 1]$, interpreted as $c_i \approx P(z_t^i = x_0^i | \mathbf{z}_t)$. The head ϕ is optimized using a Binary Cross-Entropy (BCE) loss over visible positions:

$$\mathcal{L}(\phi) = \mathbb{E}\left[\sum_{i \in \mathcal{V}_t} \text{BCE}(c_i, \mathbb{I}[z_t^i = x_0^i])\right] \quad (5)$$

where $t \sim \mathcal{U}[0, 1 - \Delta t]$, $\mathbf{x}_0 \sim \mathcal{D}$, and $\mathbf{z}_t \sim q_{\text{LBC}}(\cdot | \mathbf{x}_0, t; \theta^*, \Delta t)$ is the LBC training distribution defined in Section 3.2. Masked positions ($z_t^i = \text{M}$) contribute no loss for ϕ .

At inference time, correctness scores are converted to error scores via $e_i = 1 - c_i$, and a small subset of visible tokens with the largest e_i are selectively remasked (Section 3.3).

This design has three structural consequences. First, because θ^* is frozen, the generative ability of θ^* is preserved. Second, the head trains on errors induced by the same fixed generator used at deployment, with no generator drift during head training. Third, training only the head eliminates gradient computations in the backbone, thereby accelerating the training process by reducing both computational load and activation memory usage.

3.2 Look-back Correction

We now define the Look-back Correction (LBC) training distribution q_{LBC} referenced in Equation (5), which addresses the third design consideration in Section 2.3: evaluating earlier decisions under later denoising context. Because the reverse denoising process runs from $t = 1$ (fully masked) to $t = 0$ (fully revealed), a less corrupted state \mathbf{x}_t corresponds to a later denoising stage with richer context than a more corrupted state $\mathbf{x}_{t+t'}$.

Recall that θ^* denotes the frozen DLM parameters and Δt is the step size. For each training sample, we draw $t \sim \mathcal{U}[0, 1 - \Delta t]$ and $\mathbf{x}_t \sim q_{t|0}(\cdot | \mathbf{x}_0)$. We then sample a forward interval $t' \sim \mathcal{U}[\Delta t, 1 - t]$ to obtain a more corrupted state $\mathbf{x}_{t+t'} \sim q_{t+t'|0,t}(\cdot | \mathbf{x}_0, \mathbf{x}_t)$, and generate artifact tokens using the frozen DLM:

$$\mathbf{y} \sim p_{\theta^*}(\mathbf{x}_0 | \mathbf{x}_{t+t'}).$$

We define the set of *newly unmasked positions*—those masked in $\mathbf{x}_{t+t'}$ but visible in \mathbf{x}_t :

$$\mathcal{I}_{\text{new}} = \{i : x_{t+t'}^i = \text{M} \text{ and } x_t^i \neq \text{M}\}.$$

We select $\mathcal{M} \subseteq \mathcal{I}_{\text{new}}$ with $|\mathcal{M}| = \min(\lceil L \cdot \Delta t \rceil, |\mathcal{I}_{\text{new}}|)$ by choosing positions where the frozen model exhibits the highest prediction confidence:

$$\text{conf}_i = \max_{v \in \mathcal{V}} p_{\theta^*}(v | \mathbf{x}_{t+t'}), \quad i \in \mathcal{I}_{\text{new}},$$

following the confidence-based strategy of Nie et al. (2025). The training sequence $\mathbf{z}_t = \text{replace}(\mathbf{x}_t, \mathbf{y}, \mathcal{M})$ is formalized in Algorithm 2.

The resulting \mathbf{z}_t is a training-time proxy for a common inference scenario: tokens predicted from a more uncertain state $\mathbf{x}_{t+t'}$ persist into the later, richer context of \mathbf{x}_t . Ground-truth context in \mathbf{x}_t outside \mathcal{M} is retained so that the correction head ϕ is supervised to detect earlier mistakes by cross-referencing them with surrounding later context.

Unlike one-step artifact construction, LBC explicitly inserts predictions from a more corrupted state into a later, cleaner state, so the head is supervised to detect earlier mistakes under richer later context. We summarize the design differences between BackPlay and prior trainable self-correction methods in Table 1.

Table 1: Design comparison of trainable self-correction methods for DLMs.

	RemeDi	PRISM	BackPlay (Ours)
Trainable parameters	Full model ($\theta + \phi$)	ϕ + LoRA adapters	ϕ only (frozen θ)
Generator updated during head training	Yes (full)	Yes (LoRA)	No
Artifact source	Uniform noise	Training-time generator	Frozen deployed generator
Later-context supervision	No	No	Yes

3.3 Inference with Conservative Adaptive Remasking

We deploy (θ^*, ϕ^*) with an inference procedure that interleaves generation and correction. At each denoising step, both the generator output $p_{\theta^*}(\mathbf{x}_0 | \mathbf{x})$ and the correctness scores $\mathbf{c} = \mathbf{g}_{\theta^*, \phi^*}(\mathbf{x})$ are computed from the same forward pass on the current state \mathbf{x} , before any new tokens are revealed. For each visible position $i \in \mathcal{V} = \{j : x^{(j)} \neq \text{M}\}$, we convert

correctness scores to error scores via $e_i = 1 - c_i$. A remasking budget K and error threshold τ then select the top- K visible tokens with the highest e_i , subject to $e_i > \tau$, for remasking. Newly generated tokens in the current step are not evaluated until a later correction round, after more surrounding context has accumulated.

After remasking, the denoising timeline accounts for both the forward step and any rollback from remasking:

$$t_{\text{next}} = \max\left\{t - \Delta t + \frac{|\mathcal{M}_{\text{remask}}|}{L}, 0\right\}, \quad (6)$$

where L is the generation length. This allows the model to revisit remasked positions in subsequent steps with richer context. To avoid intervening when context is still sparse, correction is triggered only every d steps (when $N > 0$ and $N \bmod d = 0$).

The four policy hyperparameters serve distinct roles. The threshold τ controls the precision of error detection: only tokens with $e_i > \tau$ are remasked, preventing over-correction. The budget K limits the number of tokens remasked per correction round, bounding each rollback. The stride d ensures that sufficient new context accumulates between successive correction rounds. The block buffer $\mathcal{H}_{\text{block}}$ (capacity B) suppresses oscillation, as discussed below. We keep (τ, K, d, B) fixed across tasks and tokens-per-step settings; varying τ from 0.75 to 0.6 or varying B from 4 to 6 on MBPP yields a slight trade-off shift, not brittle behavior (Appendix).

Anti-Repetitive Correction. Oscillation can arise at ambiguous or weakly determined positions where the head repeatedly assigns low correctness while the generator regenerates the same token, because the surrounding context has not changed enough to alter either prediction. To prevent repeated rollback on unchanged evidence, we maintain a buffer $\mathcal{H}_{\text{block}}$ of recently remasked indices (capacity B) and temporarily exclude them from remasking candidates. This ensures the remasking budget is spent on distinct positions.

We summarize the full inference procedure in Algorithm 1.

Algorithm 1 Inference with Conservative Adaptive Remasking

Require: Frozen DLM θ^* , correction head ϕ^* , tokens per step k , generation length L , remasking budget K , error threshold τ , correction stride d , block-buffer capacity B .

- 1: $\Delta t \leftarrow k/L$, $t \leftarrow 1$, $N \leftarrow 0$, $\mathbf{x} \leftarrow [\text{MASK}]^L$, $\mathcal{H}_{\text{block}} \leftarrow \emptyset$
 - 2: **while** $t > 0$ **do**
 - 3: $\mathcal{V} \leftarrow \{i : x^{(i)} \neq [\text{MASK}]\}$; $\mathcal{M} \leftarrow \{i : x^{(i)} = [\text{MASK}]\}$; $\mathcal{M}_{\text{remask}} \leftarrow \emptyset$
 - 4: $P_{\text{demask}} \leftarrow p_{\theta^*}(\mathbf{x}_0 | \mathbf{x})$; $\mathbf{c} \leftarrow \mathbf{g}_{\theta^*, \phi^*}(\mathbf{x})$ {shared forward pass}
 - 5: $\mathcal{I} \leftarrow \text{arg-top-}k_{i \in \mathcal{M}} \left(\max_v P_{\text{demask}}^{(i)}(v) \right)$; sample $x^{(i)} \sim P_{\text{demask}}^{(i)}$ for $i \in \mathcal{I}$
 - 6: **if** $N > 0$ **and** $N \bmod d = 0$ **then**
 - 7: $\mathbf{e} \leftarrow 1 - \mathbf{c}$; $\mathcal{C} \leftarrow \mathcal{V} \setminus \mathcal{H}_{\text{block}}$ {error scores; eligible candidates}
 - 8: $\mathcal{M}_{\text{candid}} \leftarrow \text{arg-top-min}(K, |\mathcal{C}|)_{i \in \mathcal{C}}(e_i)$; $\mathcal{M}_{\text{remask}} \leftarrow \{i \in \mathcal{M}_{\text{candid}} : e_i > \tau\}$
 - 9: **for** $i \in \mathcal{M}_{\text{remask}}$ **do**
 - 10: $x^{(i)} \leftarrow [\text{MASK}]$; append i to $\mathcal{H}_{\text{block}}$; if $|\mathcal{H}_{\text{block}}| \geq B$ remove oldest
 - 11: **end for**
 - 12: **end if**
 - 13: $t \leftarrow \max\{t - \Delta t, 0\} + |\mathcal{M}_{\text{remask}}|/L$; $N \leftarrow N + 1$
 - 14: **end while**
-

4 Experiments

We evaluate BackPlay in three complementary ways: (i) a controlled frozen-vs-joint training ablation on SMDM 1B (Section 4.1), (ii) end-to-end accuracy–efficiency comparisons against SFT baselines on LLaDA 8B for coding and mathematical reasoning (Section 4.2), and (iii) controlled ablations on artifact construction (Section 4.3) and remasking policy (Section 4.4). We do not include direct reproductions of PRISM or RemeDi under matched settings; accordingly, all empirical claims are relative to the reported baselines and controls.

Throughout Section 4, we report zero-shot accuracy (Pass@1) and Iter_{avg} , the average number of DLM backbone forward passes. The correction head reuses the penultimate hidden states from the same forward pass and does not incur an additional backbone forward pass. In our LLaDA experiments, we follow the standard semi-autoregressive decoding protocol with block length 32 and maximum generation length 1024. BackPlay’s “look-back” operates over denoising-time context within this protocol, not the block length.

4.1 SMDM 1B: Controlled Ablation of Frozen vs. Joint Training

This experiment serves as a controlled ablation of optimization strategy. Following the setting in Nie et al. (2024), we adopt the 1B pretrained SMDM model as the base and perform standard SFT on augmented data (Deng et al., 2023) to obtain the finetuned model θ^* . Based on θ^* , we apply our training recipe in Section 3.1 and Section 3.2 to learn the correction head ϕ^* . As a control, we study joint optimization by training θ and ϕ simultaneously with the loss in Equation (3), denoting the final model as $(\theta + \phi)^*$.

BackPlay and the joint-training control share the same base model, training data, LBC artifact construction, correction-head architecture, and inference policy; they differ only in whether the DLM parameters θ are updated during correction-head training. We do not claim that joint optimization is universally harmful; rather, this experiment isolates the frozen-vs-joint training effect in our head-based SMDM 1B setup.

Following Section 3.1, the input to ϕ is the hidden state from the 19th transformer block (out of 20) of the SMDM 1B model. The correction head ϕ is a 2-layer transformer. For both BackPlay and the joint-training control, training sequences \mathbf{z}_t are generated using the LBC method in Section 3.2. During inference, without self-correction, all models use the confidence-based strategy in Algorithm 3 (Nie et al., 2025). With self-correction, all models adopt the conservative adaptive remasking procedure in Algorithm 1. Hyperparameters are provided in Section C.

4.1.1 Frozen vs. Joint Training on GSM8K

Table 2: Controlled ablation on GSM8K in our SMDM 1B setting. BackPlay and the joint-training control use the same LBC data construction and inference policy, and differ only in whether θ is updated during correction-head training.

Model	Acc.(No Remask)	Acc.(Remask)
SFT Baseline (θ^*)	61.33	–
Joint-Training Control ($\theta + \phi$) [*]	60.56	62.62
BackPlay (θ^*, ϕ^*)	61.33	63.46

Table 2 reports the results. As expected, freezing θ^* preserves the original no-remask accuracy of the deployed generator (61.33%), providing a sanity check that correction-head training does not alter the base model. In contrast, in our head-based SMDM 1B setup, jointly updating θ and ϕ slightly reduces no-remask accuracy to 60.56%.

With self-correction enabled, both BackPlay and the joint-training control outperform the frozen SFT baseline without self-correction, while BackPlay achieves higher accuracy than the joint-training control (63.46% vs. 62.62%). This is consistent with the hypothesis that training the head on the fixed generator that is finally deployed yields more effective correction behavior in this setting.

4.2 LLaDA 8B: End-to-End Benchmark Evaluation

To evaluate BackPlay at larger scale, we conduct experiments on LLaDA 8B (Nie et al., 2025) across coding and mathematical reasoning tasks. For coding, we use LLaDA 8B Base as the base model and perform standard SFT on the first 500,000 samples from OpenCodeInstruct (Ahmad et al., 2025) to obtain θ^* , then train the correction head ϕ^* on the same data. For math reasoning, we follow the same procedure using the first 500,000 samples from OpenMathInstruct (Toshniwal et al., 2024).

The correction head ϕ is a 3-layer Transformer that takes the output hidden state of the 31st block (out of 32) as input. Both the SFT baseline and BackPlay use the same semi-autoregressive generation protocol from LLaDA (Nie et al., 2025): block length 32, maximum generation length 1024, and early stopping upon detecting an end-of-sequence token. Unless otherwise stated, we keep the self-correction hyperparameters (τ, K, d, B) fixed across tasks and token-per-step settings. Full hyperparameters are provided in Section E.

4.2.1 Coding Experiments

We evaluate on the MBPP and HumanEval benchmarks. We observed that, across all methods, increasing the number of tokens generated per sampling step reduces Iter_{avg} but also decreases accuracy, reflecting the standard accuracy–efficiency trade-off reported in LLaDA (Nie et al., 2025).

Table 3: Coding results. BackPlay vs. SFT baseline on MBPP and HumanEval.

Method	Metric	MBPP				HumanEval			
		1	2	3	4	1	2	3	4
SFT	Acc(%)	39.8	35.6	30.4	24.6	35.98	28.66	24.39	20.73
	Iter_{avg}	119.4	59.3	44.3	30.0	131.0	67.1	41.5	29.2
BackPlay	Acc(%)	40.2	40.0	35.8	33.8	36.59	33.54	33.29	27.44
	Iter_{avg}	134.0	69.6	45.6	35.9	138.6	71.1	41.5	35.5

Table 3 summarizes the results. BackPlay consistently improves the accuracy–efficiency trade-off: at more aggressive multi-token decoding settings, BackPlay maintains higher accuracy than the SFT baseline at comparable or moderately larger decoding budgets. On MBPP, BackPlay with 2 tokens per step reaches 40.0% accuracy, exceeding the baseline at 1 token per step (39.8%) while reducing Iter_{avg} from 119.4 to 69.6—a 41.7% reduction. On HumanEval, BackPlay with 3 tokens per step attains 33.29%, exceeding the baseline at 2 tokens per step (28.66%) while reducing Iter_{avg} from 67.1 to 41.5.

BackPlay is primarily intended for multi-token decoding regimes, where dependency errors are more prevalent. At the slowest setting (1 token per step), the corrector can still improve accuracy, but the additional intervention opportunities may increase Iter_{avg} . Figure 1 visualizes the trade-off relative to the SFT baseline on one representative coding benchmark (MBPP) and one representative reasoning benchmark (GSM8K); full numerical results for HumanEval and MATH are reported in Tables 3 and 4.

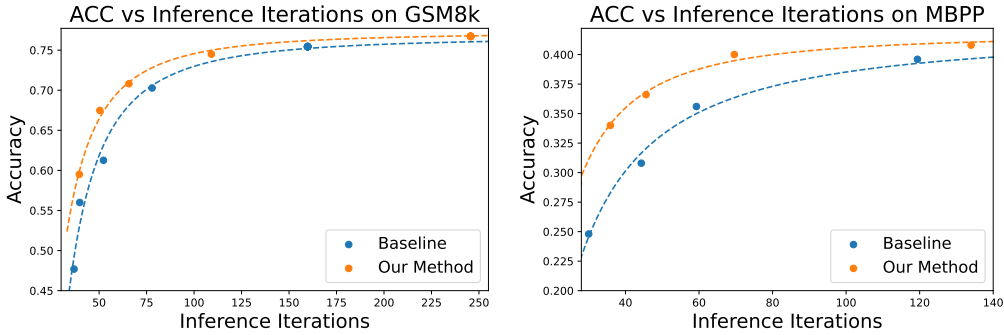


Figure 1: Plot of Accuracy vs. Iter_{avg} for BackPlay and the SFT baseline on GSM8K and MBPP. Data from Tables 3 and 4. BackPlay improves the accuracy–efficiency trade-off under multi-token decoding.

4.2.2 Mathematical Reasoning Experiments

We evaluate zero-shot accuracy (Pass@1) on GSM8K (Cobbe et al., 2021) and MATH (Hendrycks et al., 2021). Table 4 shows that BackPlay consistently improves the accuracy–efficiency trade-off over the SFT baseline in the reported mathematical reasoning settings.

On GSM8K, BackPlay with 3 tokens per step reaches 70.81%, exceeding the baseline at 2 tokens per step (70.28%) while reducing Iter_{avg} from 77.9 to 65.7—a 15.7% reduction. On MATH, BackPlay with 3 tokens per step reaches 33.6%, exceeding the baseline at 2 tokens per step (31.6%) while reducing Iter_{avg} from 85.3 to 75.4. As in the coding experiments, the benefit is most pronounced under multi-token decoding.

Table 4: Math reasoning results. BackPlay vs. SFT baseline on GSM8K and MATH.

Method	Metric	GSM8K					MATH			
		1	2	3	4	5	1	2	3	4
SFT	Acc(%)	75.44	70.28	61.26	56.18	47.69	34.2	31.6	28.4	22.4
	Iter_{avg}	159.8	77.9	52.3	39.8	36.8	190.5	85.3	61.1	47.1
BackPlay	Acc(%)	76.72	74.30	70.81	67.48	59.51	36.2	34.0	33.6	28.4
	Iter_{avg}	245.6	109.1	65.7	50.4	39.6	324.42	127.9	75.4	56.1

4.3 Controlled Ablation on Artifact Source

To evaluate the importance of realistic artifact construction, we conduct a controlled ablation: while maintaining the training recipe in Section 3.1, we replace the model-generated artifacts in LBC (Section 3.2) with a uniform distribution over the vocabulary, re-train the correction head, and re-evaluate under the same inference policy. This experiment is not a full reproduction of RemeDi; it is a controlled artifact-source ablation that keeps the backbone, head architecture, training recipe, and inference policy fixed and changes only the artifact source. We evaluate on MBPP and GSM8K under the LLaDA 8B setting described in Section 4.2.

Table 5: Uniform-artifact control on MBPP and GSM8K.

Method	Metric	MBPP				GSM8K				
		1	2	3	4	1	2	3	4	5
Unif. Artifact	Acc(%)	40.0	37.6	33.8	29.8	75.74	70.74	63.61	58.38	49.37
	Iter_{avg}	119.2	60.4	44.1	29.6	158.1	78.6	52.7	40.5	36.4
BackPlay	Acc(%)	40.2	40.0	35.8	33.8	76.72	74.30	70.81	67.48	59.51
	Iter_{avg}	134.0	69.6	45.6	35.9	245.6	109.1	65.7	50.4	39.6

Table 5 and Figure 2 show that replacing model-generated artifacts with uniform noise consistently shifts the accuracy–iteration curve downward across both benchmarks, supporting the importance of realistic, model-generated artifact construction for effective self-correction.

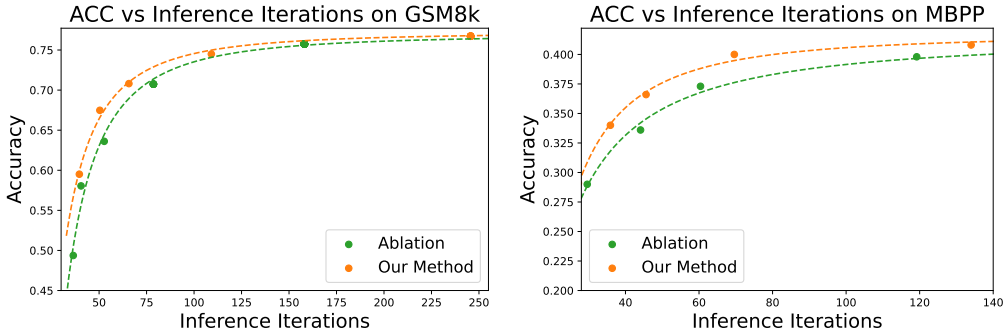


Figure 2: Accuracy vs. Iter_{avg} : BackPlay vs. the uniform-artifact control on GSM8K and MBPP. Replacing model-generated artifacts with uniform noise consistently shifts the curve downward. Data from Table 5.

4.4 Random-Remask Control

We compare BackPlay’s learned remasking policy against a random-remask control. Specifically, we replace the error scores e_i in the conservative adaptive remasking procedure

Table 6: Random-remask control on GSM8K.

Method	Metric	1	2	3	4	5
Rand.	Acc(%)	75.82	71.95	66.64	63.08	51.10
	Iter _{avg}	338.4	155.6	75.3	58.7	40.9
BackPlay	Acc(%)	76.72	74.30	70.81	67.48	59.51
	Iter _{avg}	245.6	109.1	65.7	50.4	39.6

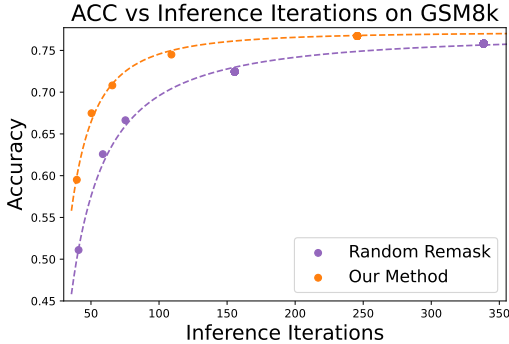


Figure 3: Accuracy vs. Iter_{avg}: BackPlay vs. random-remask on GSM8K. Data from Table 6.

(Algorithm 1) with independent random values sampled from $U[0, 1]$, so that tokens are selected for remasking uniformly at random rather than by learned correctness scores. All other hyperparameters remain identical. Because our decoding protocol differs from Wang et al. (2025), this experiment should be interpreted as a random-remask control within our inference framework rather than an exact reproduction of their full method.

Although random remasking also improves accuracy over the SFT baseline, it cannot target erroneous tokens accurately, leading to unnecessary masking of correct tokens and redundant regeneration that increases Iter_{avg}. As shown in Table 6 and Figure 3, across all reported token-per-step settings on GSM8K, BackPlay achieves both higher accuracy and fewer DLM forward passes than the random-remask control. The gap indicates that the gain comes from targeted error selection rather than from simply remasking more tokens.

5 Conclusion

We propose BackPlay, a head-only self-correction framework for frozen finetuned Diffusion Language Models. BackPlay decouples corrector training from the generator: the finetuned DLM remains frozen, and only a lightweight correction head is trained on errors produced by the same fixed generator used at deployment, avoiding generator drift during head training. We introduce Look-back Correction, a training mechanism that injects predictions from earlier, more corrupted denoising states into later, richer contexts, enabling the head to leverage later context to detect earlier mistakes. At inference time, BackPlay converts the learned correctness scores into a conservative remasking policy that periodically revisits previously generated tokens. Experiments on mathematical reasoning and code generation benchmarks show that BackPlay improves the speed–quality trade-off of the underlying DLM under multi-token decoding.

References

Wasi Uddin Ahmad, Aleksander Ficek, Mehrzad Samadi, Jocelyn Huang, Vahid Noroozi, Somshubra Majumdar, and Boris Ginsburg. OpenCodeInstruct: A large-scale instruction tuning dataset for code LLMs. *arXiv preprint arXiv:2504.04030*, 2025.

Jacob Austin, Daniel D. Johnson, Jonathan Ho, Daniel Tarlow, and Rianne van den Berg. Structured denoising diffusion models in discrete state-spaces. *Advances in neural information processing systems*, 34:17981–17993, 2021.

- Karl Cobbe, Vineet Kosaraju, Mohammad Bavarian, Mark Chen, Heewoo Jun, Lukasz Kaiser, Matthias Plappert, Jerry Tworek, Jacob Hilton, Reiichiro Nakano, et al. Training verifiers to solve math word problems. *arXiv preprint arXiv:2110.14168*, 2021.
- Yuntian Deng, Kiran Prasad, Roland Fernandez, Paul Smolensky, Vishrav Chaudhary, and Stuart Shieber. Implicit chain of thought reasoning via knowledge distillation. *arXiv preprint arXiv:2311.01460*, 2023.
- Itai Gat, Tal Remez, Neta Shaul, Felix Kreuk, Ricky TQ Chen, Gabriel Synnaeve, Yossi Adi, and Yaron Lipman. Discrete flow matching. *Advances in Neural Information Processing Systems*, 37:133345–133385, 2024.
- Zhengfu He, Tianxiang Sun, Qiong Tang, Kuanning Wang, Xuanjing Huang, and Xipeng Qiu. DiffusionBERT: Improving generative masked language models with diffusion models. In *Proceedings of the 61st annual meeting of the association for computational linguistics (volume 1: Long papers)*, pp. 4521–4534, 2023.
- Dan Hendrycks, Collin Burns, Saurav Kadavath, Akul Arora, Steven Basart, Eric Tang, Dawn Song, and Jacob Steinhardt. Measuring mathematical problem solving with the MATH dataset. *arXiv preprint arXiv:2103.03874*, 2021.
- Zemin Huang, Yuhang Wang, Zhiyang Chen, and Guo-Jun Qi. Don’t settle too early: Self-reflective remasking for diffusion language models. *arXiv preprint arXiv:2509.23653*, 2025.
- Wonjun Kang, Kevin Galim, Seunghyuk Oh, Minjae Lee, Yuchen Zeng, Shuibai Zhang, Coleman Hooper, Yuezhou Hu, Hyung Il Koo, Nam Ik Cho, et al. ParallelBench: Understanding the trade-offs of parallel decoding in diffusion LLMs. *arXiv preprint arXiv:2510.04767*, 2025.
- Jaeyeon Kim, Seunggeun Kim, Taekyun Lee, David Z Pan, Hyeji Kim, Sham Kakade, and Sitan Chen. Fine-tuning masked diffusion for provable self-correction. *arXiv preprint arXiv:2510.01384*, 2025.
- Anji Liu, Oliver Broadrick, Mathias Niepert, and Guy Van den Broeck. Discrete copula diffusion. *arXiv preprint arXiv:2410.01949*, 2024.
- Aaron Lou, Chenlin Meng, and Stefano Ermon. Discrete diffusion modeling by estimating the ratios of the data distribution. *arXiv preprint arXiv:2310.16834*, 2023.
- Shen Nie, Fengqi Zhu, Chao Du, Tianyu Pang, Qian Liu, Guangtao Zeng, Min Lin, and Chongxuan Li. Scaling up masked diffusion models on text. *arXiv preprint arXiv:2410.18514*, 2024.
- Shen Nie, Fengqi Zhu, Zebin You, Xiaolu Zhang, Jingyang Ou, Jun Hu, Jun Zhou, Yankai Lin, Ji-Rong Wen, and Chongxuan Li. Large language diffusion models. *arXiv preprint arXiv:2502.09992*, 2025.
- Fred Zhangzhi Peng, Zachary Bezemek, Sawan Patel, Jarrid Rector-Brooks, Sherwood Yao, Avishek Joey Bose, Alexander Tong, and Pranam Chatterjee. Path planning for masked diffusion model sampling. *arXiv preprint arXiv:2502.03540*, 2025.
- Subham Sekhar Sahoo, Marianne Arriola, Yair Schiff, Aaron Gokaslan, Edgar Marroquin, Justin T. Chiu, Alexander Rush, and Volodymyr Kuleshov. Simple and effective masked diffusion language models. *Advances in Neural Information Processing Systems*, 37:130136–130184, 2024.
- Jiaxin Shi, Kehang Han, Zhe Wang, Arnaud Doucet, and Michalis K. Titsias. Simplified and generalized masked diffusion for discrete data. *Advances in neural information processing systems*, 37:103131–103167, 2024.
- Shubham Toshniwal, Wei Du, Ivan Moshkov, Branislav Kisacanian, Alexan Ayrapetyan, and Igor Gitman. OpenMathInstruct-2: Accelerating AI for math with massive open-source instruction data. *arXiv preprint arXiv:2410.01560*, 2024.

Hugo Touvron, Louis Martin, Kevin Stone, Peter Albert, Amjad Almahairi, Yasmine Babaei, Nikolay Bashlykov, Soumya Batra, Prajjwal Bhargava, Shruti Bhosale, et al. Llama 2: Open foundation and fine-tuned chat models. *arXiv preprint arXiv:2307.09288*, 2023.

Guanghan Wang, Yair Schiff, Subham Sekhar Sahoo, and Volodymyr Kuleshov. Remasking discrete diffusion models with inference-time scaling. *arXiv preprint arXiv:2503.00307*, 2025.

Minkai Xu, Tomas Geffner, Karsten Kreis, Weili Nie, Yilun Xu, Jure Leskovec, Stefano Ermon, and Arash Vahdat. Energy-based diffusion language models for text generation. *arXiv preprint arXiv:2410.21357*, 2024.

Jiacheng Ye, Zhihui Xie, Lin Zheng, Jiahui Gao, Zirui Wu, Xin Jiang, Zhenguo Li, and Lingpeng Kong. Dream 7B: Diffusion large language models. *arXiv preprint arXiv:2508.15487*, 2025.

Yixiu Zhao, Jiaxin Shi, Feng Chen, Shaul Druckmann, Lester Mackey, and Scott Linderman. Informed correctors for discrete diffusion models. *arXiv preprint arXiv:2407.21243*, 2024.

Fengqi Zhu, Rongzhen Wang, Shen Nie, Xiaolu Zhang, Chunwei Wu, Jun Hu, Jun Zhou, Jianfei Chen, Yankai Lin, Ji-Rong Wen, et al. LLaDA 1.5: Variance-reduced preference optimization for large language diffusion models. *arXiv preprint arXiv:2505.19223*, 2025.

A Implementation Details of LBC

We summarize the Look-back Correction algorithm in Algorithm 2.

Algorithm 2 Look-back Correction (LBC) Training Recipe

- 1: **Input:** Clean data \mathbf{x}_0 , frozen DLM parameters θ^* , step size Δt , sequence length L
 - 2: Sample time step $t \sim \mathcal{U}[0, 1 - \Delta t]$
 - 3: Sample state $\mathbf{x}_t \sim q_{t|0}(\cdot | \mathbf{x}_0)$
 - 4: Sample forward interval $t' \sim \mathcal{U}[\Delta t, 1 - t]$
 - 5: Sample more corrupted state $\mathbf{x}_{t+t'} \sim q_{t+t'|0,t}(\cdot | \mathbf{x}_0, \mathbf{x}_t)$
 - 6: Generate artifact sequence: $\mathbf{y} \sim p_{\theta^*}(\mathbf{x}_0 | \mathbf{x}_{t+t'})$
 - 7: Identify newly unmasked positions: $\mathcal{I}_{\text{new}} = \{i : x_{t+t'}^i = [\text{MASK}] \text{ and } x_t^i \neq [\text{MASK}]\}$
 - 8: Calculate subset size: $k = \min(\lceil L \cdot \Delta t \rceil, |\mathcal{I}_{\text{new}}|)$
 - 9: Select top- k confident indices from \mathcal{I}_{new} :
 $\mathcal{M} = \text{arg-top-}k_{i \in \mathcal{I}_{\text{new}}}(\max_v p_{\theta^*}(v | \mathbf{x}_{t+t'}))$
 - 10: Construct training sequence: $\mathbf{z}_t = \text{replace}(\mathbf{x}_t, \mathbf{y}, \mathcal{M})$
 - 11: **Return:** Training pair $(\mathbf{z}_t, \mathbf{x}_0)$
-

B Training Details on SMDM 1B

For the SFT stage, we use the 1B pretrained model from SMDM (Nie et al., 2024) as the base model and train on the augmented data from Deng et al. (2023). Following Nie et al. (2024), we initially train for 40 epochs, then extend to 80 epochs after observing continued accuracy gains on GSM8K. The training configuration is listed in Table 7.

Table 7: SFT configuration for SMDM 1B.

Base Model	
Architecture	SMDM (Nie et al., 2024)
Parameters	1028M
Tokenizer	LLaMA2 Tokenizer (Touvron et al., 2023)
Training	
Sequence Length	256
Optimizer	AdamW
Learning Rate	2×10^{-4}
Weight Decay	0.1
Global Batch Size	256
β_1	0.9
β_2	0.95
Warmup Ratio	0.01
Learning Rate Schedule	cosine

The correction head is trained on the same augmented data for 20 epochs. The training configuration is summarized in Table 8. For the joint-training control, we use the same hyperparameters as SFT (Table 7) and tune $\gamma \in \{0.01, 0.1, 0.5\}$, reporting the best result.

C Inference Details on SMDM 1B

For inference without remasking, following the setting in SMDM and LLaDA (Nie et al., 2025), we use the confidence-based strategy shown in Algorithm 3: at each iteration, the top- k masked positions with the highest predicted confidence are demasked. For inference with remasking, both BackPlay and the joint-training control use the conservative adaptive remasking procedure in Algorithm 1. Hyperparameters are summarized in Table 9.

Table 8: Correction head training config for SMDM 1B.

Model	
Architecture	2-layer Transformer
Parameters	90M
Training	
Step Size Δt in LBC	$\frac{1}{32}$
Sequence Length	256
Optimizer	AdamW
Learning Rate	2×10^{-3}
Weight Decay	0.1
Global Batch Size	256
β_1	0.9
β_2	0.95
Warmup Ratio	0.01
Learning Rate Schedule	cosine

Table 9: Inference config for SMDM 1B.

Inference	
Generation Length	256
Tokens per step k	2
Conservative Adaptive Remasking	
Error threshold τ	0.75
Remasking budget K	2
Correction stride d	4
Block buffer B	4

Algorithm 3 Confidence-based inference strategy from LLaDA (Nie et al., 2025)

Require: Generative model θ^* , tokens per step k , generation length L .

- 1: $\Delta t \leftarrow \frac{k}{L}$, $\mathbf{x}_1 \leftarrow [\text{MASK}]^L$, $t \leftarrow 1$, $N \leftarrow 0$
- 2: **while** $t > 0$ **do**
- 3: $t_{\text{new}} \leftarrow \max\{t - \Delta t, 0\}$, $x_{t_{\text{new}}} \leftarrow x_t$, $\mathcal{M} \leftarrow \{i \mid x_t^{(i)} = [\text{MASK}]\}$
- 4: $P_{\text{demask}} \leftarrow p_{\theta^*}(\mathbf{x}_0 \mid \mathbf{x}_t)$
- 5: $\mathcal{I} \leftarrow \text{arg-top-}k_{i \in \mathcal{M}} \left(P_{\text{demask}}^{(i)} \right)$
- 6: Sample $\mathbf{x}_{t_{\text{new}}}[i] \sim P_{\text{demask}}[i]$ for all $i \in \mathcal{I}$
- 7: $t \leftarrow t_{\text{new}}$, $N \leftarrow N + 1$
- 8: **end while**

D Training Details on LLaDA 8B

D.1 Supervised Finetuning (SFT)

Our SFT procedure for LLaDA 8B Base follows Nie et al. (2025). We set the maximum sequence length to 1024 and pad all sequences to this length using the end-of-sequence token [EoS].

In LLaDA (Nie et al., 2025), padding [EoS] tokens are treated as normal tokens and randomly masked with the same probability as response tokens. However, when most training sequences are much shorter than the maximum length, the abundance of [EoS] tokens causes the model to predict [EoS] with high probability, leading to premature termination of generation. This issue is also noted in the LLaDA codebase.

To address this, we apply a simple modification during SFT: the first 16 [EoS] tokens after the response are treated as normal tokens and may be masked, while all remaining [EoS] padding tokens are kept unmasked. This effectively limits the number of [EoS] tokens the model must predict and resolves the early-termination issue.

We use the standard demasking loss (Equation (1)) and train LLaDA 8B Base on the first 500,000 samples from OpenCodeInstruct (Ahmad et al., 2025) for coding experiments (Section 4.2.1) and the first 500,000 samples from OpenMathInstruct (Toshniwal et al., 2024) for math reasoning experiments (Section 4.2.2). Hyperparameters are summarized in Table 10.

D.2 Training of the correction head

The correction head is trained after the SFT stage, with the DLM parameters θ^* frozen. We use a 3-layer Transformer block as the correction head ϕ , taking the output of the 31st layer

Table 10: SFT configuration for LLaDA 8B.

Base Model	
Architecture	LLaDA Base (Nie et al., 2025)
Parameters	8B
Tokenizer	LLaDA Tokenizer (Nie et al., 2025)
Training	
Sequence Length	1024
Optimizer	AdamW
Learning Rate	2.5×10^{-5}
Weight Decay	0.1
Global Batch Size	256
β_1	0.9
β_2	0.95
Warmup Ratio	0.01
Learning Rate Schedule	cosine

of the DLM (out of 32 layers) as input. The head outputs a correctness score $c_i \in [0, 1]$ for each visible position, estimating $P(z_t^i = x_0^i \mid \mathbf{z}_t)$. The correction head has approximately 600M parameters, substantially smaller than the 8B base model. The training procedure follows Section 3.1 and Section 3.2, using the same dataset as for θ^* (Section D.1). Consistent with the SFT stage, the first 16 [EoS] tokens are treated as normal tokens, and remaining [EoS] padding tokens are kept unmasked during the construction of \mathbf{z}_t (Equation (5)). Hyperparameters are summarized in Table 11.

D.3 Training details of the ablation study

For the artifact-source ablation in Section 4.3, we retrain only the correction head on the modified training data (uniform artifacts instead of model-generated artifacts). All training and inference hyperparameters remain identical to those in Section D.2.

Table 11: Correction head training config for LLaDA 8B.

Model	
Architecture	3-layer Transformer
Parameters	$\sim 600\text{M}$
Training	
Step Size Δt in LBC	$\frac{1}{64}$
Sequence Length	1024
Optimizer	AdamW
Learning Rate	5×10^{-4}
Weight Decay	0.1
Global Batch Size	256
β_1	0.9
β_2	0.95
Warmup Ratio	0.01
Learning Rate Schedule	cosine

Table 12: Inference config for LLaDA 8B.

Inference	
Generation Length	1024
Tokens per step k	–
Conservative Adaptive Remasking	
Error threshold τ	0.75
Remasking budget K	2
Correction stride d	4
Block buffer B	4

E Inference Details on LLaDA 8B

For the SFT baseline, we use the confidence-based strategy from LLaDA (Algorithm 3). For BackPlay, we use the conservative adaptive remasking procedure in Algorithm 1. Tokens per step k is varied across experiments to compare the accuracy–efficiency trade-off, as discussed in Section 4 and reported in the result tables. All other inference hyperparameters are summarized in Table 12. For the random-remask control (Section 4.4), all hyperparameters are kept identical to those of BackPlay, except that the error scores e_i are replaced with independent random values sampled from $U[0, 1]$.

E.1 Sensitivity to remasking threshold τ

To examine the sensitivity of the error threshold τ , we run an additional inference experiment with $\tau = 0.6$ while keeping all other hyperparameters identical to Table 12, and evaluate on MBPP. As shown in Table 13, lowering τ slightly increases accuracy at larger tokens-per-step settings but also increases Iter_{avg} , reflecting a standard precision–recall trade-off in error detection rather than brittle behavior.

Table 13: Sensitivity of τ on MBPP. Lowering τ from 0.75 to 0.6 yields a modest accuracy–iteration trade-off.

Method	Tokens/Step	Acc(%)	Iter_{avg}
$\tau = 0.6$	1	40.2	138.2
	2	40.0	71.6
	3	36.4	48.2
	4	34.2	36.4
$\tau = 0.75$	1	40.2	134.0
	2	40.0	69.6
	3	35.8	45.6
	4	33.8	35.9

E.2 Sensitivity to Block buffer B

To examine the sensitivity of the Block buffer B , we run an additional inference experiment with $B = 6$ while keeping all other hyperparameters identical to Table 12, and evaluate on MBPP. As shown in Table 14, setting $B = 6$ only has a very slight impact on the final result.

Table 14: Sensitivity of B on MBPP. Increasing B from 4 to 6 only has a very slight impact.

Method	Tokens/Step	Acc(%)	Iter_{avg}
$B = 6$	1	40.2	132.4
	2	39.8	68.8
	3	35.8	45.4
	4	33.8	35.8
$B = 4$	1	40.2	134.0
	2	40.0	69.6
	3	35.8	45.6
	4	33.8	35.9